

# Specific Adsorption of Halide Ions on Iron Surface: A Combined Electrochemical and Monte Carlo Simulation Investigation

Lei Guo<sup>1,\*</sup>, Yiman Ou<sup>1</sup>, Xun Shen<sup>1</sup>, Savaş Kaya<sup>2</sup>, Wei Shi<sup>1</sup>, Renhui Zhang<sup>1</sup>, Xingwen Zheng<sup>3</sup>, Junjun Wang<sup>4</sup>

<sup>1</sup> School of Material and Chemical Engineering, Tongren University, Tongren 554300, China

<sup>2</sup> Department of Chemistry, Faculty of Science, Cumhuriyet University, Sivas 58140, Turkey

<sup>3</sup> Material Corrosion and Protection Key Laboratory of Sichuan province, Zigong 643000, China

<sup>4</sup> College of Materials Science and Engineering, Chongqing University of Technology, Chongqing 400054, China

\*E-mail: [cqglei@163.com](mailto:cqglei@163.com)

Received: 7 April 2017 / Accepted: 22 May 2017 / Published: 12 July 2017

---

The specific adsorption effect of halide ions (*i.e.*, Cl<sup>-</sup>, Br<sup>-</sup>, I<sup>-</sup>) on the surface of mild steel in acid media has been explored by electrochemical and Monte Carlo simulating methods. The electrochemical impedance spectroscopy (EIS) and Tafel polarization results demonstrated that the mild steel was protected from corrosion to some extent when KX (X=Cl, Br, I) exist. The adsorption strength was determined by calculating a customized parameter, namely, adsorption efficiency, which suggests that adsorption ability, in descending order of magnitude, was I<sup>-</sup>, Br<sup>-</sup>, and Cl<sup>-</sup>. Moreover, Monte Carlo simulation was employed to look for the most stable adsorption configurations of halide ions onto Fe(110) surface. Our experimental findings were in accordance with the theoretical analysis.

---

**Keywords:** Halide ions, Specific adsorption, Iron surface, Electrochemical, Monte Carlo simulation

## 1. INTRODUCTION

Toward understanding the structural characteristics of the metal/electrolyte interface is very critical in fields of electrochemical research. Especially, the adsorption phenomenon of halide anions has captured the attention of researchers for several reasons, including relatively small volume and strong adsorption ability [1-4]. Actually, the specific adsorption of anions on different electrode surface has been widely reported. For instance, Larkin et al. [5] have studied the specific adsorption of

$\text{Cl}^-$ ,  $\text{Br}^-$ ,  $\text{I}^-$ , azide, and thiocyanate on electropolished polycrystalline Ag/aqueous interface using various capacitance measurements. Toshima and Uchida [6] reported the specific effect of halide ions at the Ge/electrolyte interface with the frequency dispersion of the interfacial impedance approach. On the other hand, Ha and co-workers [7] found that the specific adsorption of halide ions can have an important influence on the controlled syntheses of different shaped gold nano components, such as nanoprisms and nanorods. Some researchers reported that the specific adsorption of fluorine ion inside the double layer was helpful for increasing catalytic activity for oxygen reduction/evolution reactions at  $\alpha\text{-MnO}_2$  electrodes [8].

Recently, the use of corrosion inhibitor has been a hot research topic in metal corrosion and protection. Many studies showed that there existed synergistic effect between the inhibitor molecules and KI [9-11]. There is also evidence that some inhibitors exhibit more efficiency in HCl solution than that in  $\text{H}_2\text{SO}_4$  solution [12-14]. As has been pointed out in our previous work, some substances that containing halide ions in their own structures usually show excellent corrosion inhibition properties. Such as the surfactant benzalkonium chloride [15], as well as the ionic liquid 1-butyl-3-methyl-1H-benzimidazolium iodide [16]. As depicted in Figure 1, these phenomena can all be attributed to the specific adsorption of anions, and especially the halide ions have a great influence on the inhibiting behaviors of organics. However, there are lack of systematic studies on the adsorption mechanism of anions at molecular or atomic level. Fortunately, with the development of computer technology, molecular modeling method has been widely used to explain some experimental phenomena, on account of that it is an effective, reliable, advanced and less time-consuming approach.

In this work, the adsorption behavior of three halide ions, that is  $\text{Cl}^-$ ,  $\text{Br}^-$ ,  $\text{I}^-$ , on the surface of mild steel in 0.5 M  $\text{H}_2\text{SO}_4$  medium has been systematically researched by electrochemistry test and Monte Carlo simulation technique. The adsorption mechanism was highlighted by fitting the impedance as well as Tafel results, and the experimental results were further confirmed by theoretical simulations.

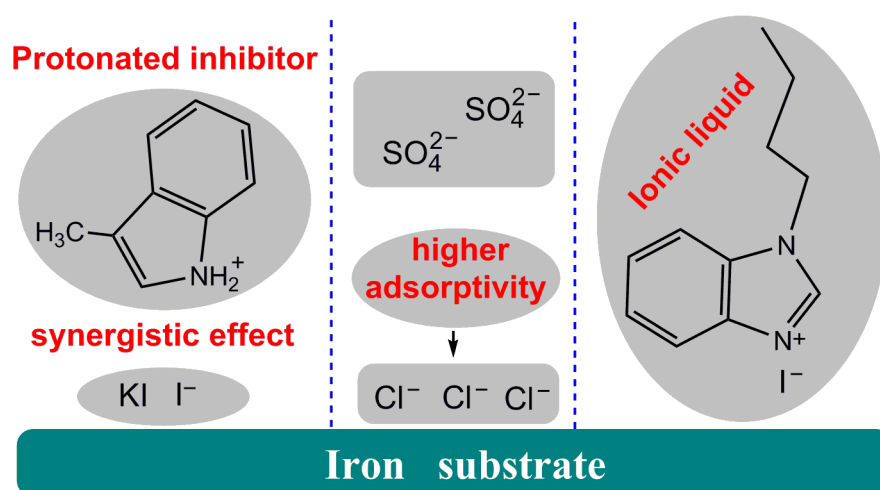


**Figure 1.** Schematic diagram showing some typical situations that containing halide ions in inhibitor research.

## 2. EXPERIMENTAL DETAILS

### 2.1. Materials and chemicals

The mild steel (Q235A) specimens were selected as the working electrode. Its chemical composition is given in Table 1, and the appearance of our homemade Q235A electrode is shown in Figure 2. As shown, the cube steel rod was inserted in epoxy resin with a plastic pipe as its shell, and a surface area of  $1.0 \times 1.0 \text{ cm}^2$  was exposed to the electrolyte solution. Before each test, the electrode was mechanically abraded with a series emery papers (200, 400, 600, 800, and 1500 grit size), washed thoroughly with distill water, degreased and cleaned ultrasonically with ethanol, dried under hot air blower and stored in desiccators. The electrolyte solution was 0.5 M  $\text{H}_2\text{SO}_4$ , prepared by using 98%  $\text{H}_2\text{SO}_4$  of analytical grade and doubly distilled water. Potassium iodide, potassium bromide, and potassium chloride were purchased from Aladdin company (Shanghai, China). All chemicals were used as received.

**Table 1.** Chemical composition of Q235A mild steel.

Element	C	Mn	Si	P	S	Fe
wt%	0.22	1.40	0.35	0.045	0.05	balance

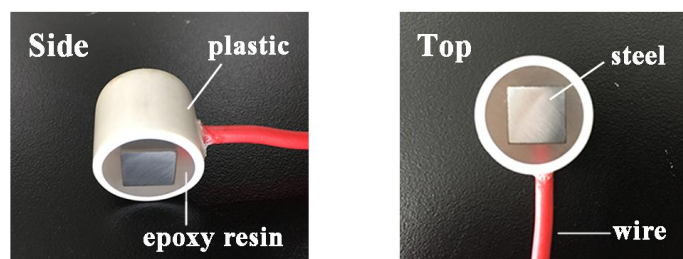


**Figure 2.** Side and top views of the Q235A electrode prepared in our laboratory.

### 2.2. Electrochemical measurements

All the electrochemical measurements were performed in a laboratory-made three-electrode thermostated cell, and the RST5000F electrochemical workstation (purchased from Zhengzhou Shiruisi Instrument Technology Co. Ltd., China) was employed. The testing temperature was controlled at  $298 \pm 1 \text{ K}$  and under ambient conditions. A platinum disk was used as counter electrode, and a saturated calomel electrode (SCE) coupled with a Luggin-Haber capillary as the reference electrode. All potentials are referred to SCE electrode. During the tests, the tip of the Luggin capillary should be very close to the surface of the Q235A electrode so as to reduce liquid-junction potential and solution resistance. Prior to each measurement, a stabilization period of 1 h was allowed, which was proved to be sufficient for the open circuit corrosion potential ( $E_{\text{ocp}}$ ) to attain the steady state. The impedance data was measured and collected under corrosion potential in the frequency range from 100

kHz to 5 mHz, and the ac amplitude was 10 mV. The obtained EIS data were fitted using the ZsimpWin 3.00 software (EG&G, USA). In the potentiodynamic polarization test, the electrode potential has been changed automatically in the potential range of  $\pm 250$  mV vs  $E_{ocp}$ , and the scan rate was 0.5 mV/s. In order to obtain reproducible results, each experiment was repeated at least three times.

### 2.3. Calculation method

The adsorption behavior of halide ions  $X^-$  ( $X=Cl, Br, I$ ) on iron surface was studied by performing Monte Carlo (MC) simulations using Adsorption Locator module from BIOVIA company. The simulated annealing task was performed, in which a substrate loaded with a certain number of adsorbates can be simulated, and the most stable adsorption sites were determined by repeatedly searching the configurational space of the substrate-adsorbate system with the decrease of temperature. The Metropolis Monte Carlo approach [17] was adopted, which identifies the structures in an ensemble by producing a series of configurations,  $m, n, \dots$ , and the transition probability from  $m$  to  $n$  is  $\pi_{mn}$ . Therefore, when configuration  $m$  is sampled with a frequency  $\rho_m$ ,  $\rho_m \pi_{mn}$  of them will be transformed to  $n$  on average. Similarly,  $\rho_n \pi_{nm}$  of configurations  $n$  are converted to  $m$ . In the MC simulation, the adsorbate components seek to be optimal on the clean metal surface by suffering random rotation and translation until they satisfy certain convergence criteria. The Metropolis method assumes that the adsorbates possess rigid structures, poor torsional flexibility, and the internal degrees of freedom for the components is also ignored. More details about the aspects of Monte Carlo simulations can be seen elsewhere [18-21].

Besides, the COMPASSII [22] force field was used, and the Fe(110) plane was selected as simulated surface in view of its stability character [23]. A  $1 \times 1$  unit-cell with five-layer was first cleaved from pure  $\alpha$ -Fe crystal, and then was enlarged to a  $5 \times 5$  supercell. After that, a vacuum slab with 30 Å thickness was built above the Fe(110). The halide ions  $X^-$  were made to adsorb on the built Fe(110) surface to obtain the most stable adsorption configurations of  $X^-/Fe(110)$  systems. The van der Waals and electrostatic interactions were handled with atom-based and Ewald summation method, respectively, with a cutoff radius of 18.5 Å, spline width 1.0 Å. The number of temperature cycles was set as ten and  $10^5$  steps per cycle. Ultimately, we can obtain the related energy parameters for the adsorption systems.

## 3. RESULTS AND DISCUSSION

### 3.1. EIS studies

Nyquist and bode plots of mild steel in 0.5 M  $H_2SO_4$  solution in the absence and presence of  $5 \times 10^{-3}$  M  $KX$  ( $X=Cl, Br, I$ ) are represented in Figure 3. We can see that the Nyquist plots are characterized by one flattened semicircle corresponding to one time constant in bode-phase plots, with the centre under the real axis. The capacitive loops suggest that the charge transfer controls the corrosion processes [24], and they are not ideal semicircles, which can be ascribed to the frequency

dispersion effect resulting from electrode roughness, grain boundaries, inhomogeneous conductivity, diffusion, or adsorption of ions [25-27]. The high frequency part in the impedance and phase angle curves shows the characteristic of heterogeneous surface layer, while the low frequency part represents the kinetic response to the charge transfer process. On the other hand, it can be concluded that the diameter of the capacitive reactance arc, the impedance of the double layer, as well as the maximum phase angle all increase gradually with the additive from KCl to KI. This means that a strong and compact absorption layer can be formed on the steel surface.

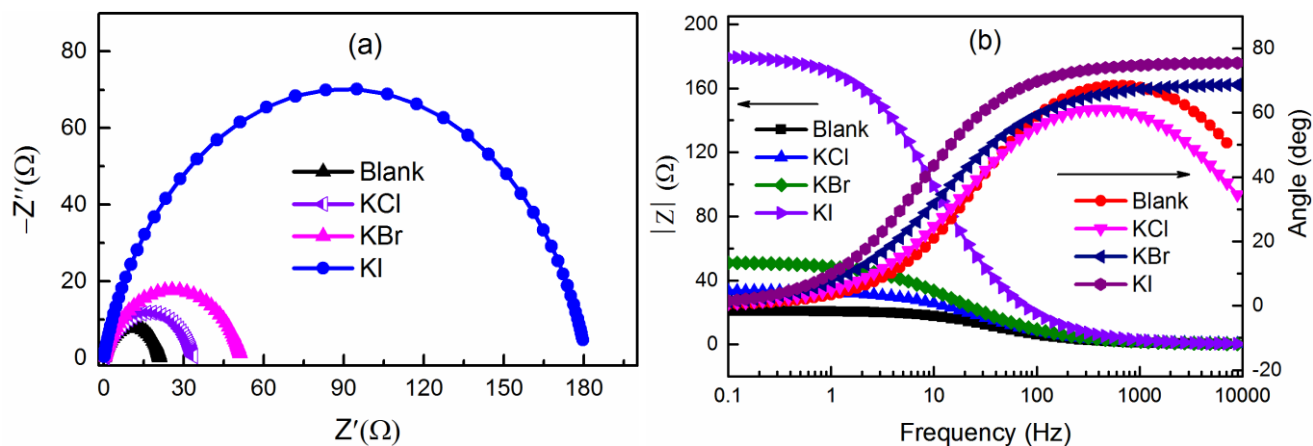


**Figure 3.** Experimental Nyquist (a) and Bode (b) plots for mild steel in 0.5 M  $\text{H}_2\text{SO}_4$  with and without  $5 \times 10^{-3}$  M KX (X=Cl, Br, I).

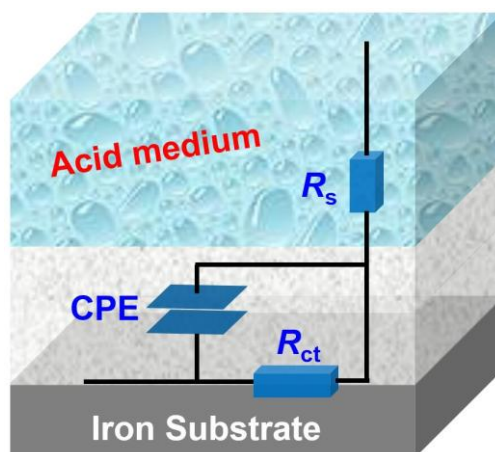


**Figure 4.** Equivalent circuit that models the metal/solution interface.

Because of the non-ideal behavior of the mild steel/acid interface, a constant phase element (CPE) was introduced to estimate the frequency-distributed double-layer capacitance. As depicted in Figure 4, a Randles equivalent circuit model was used.  $R_s$  is the solution resistance, and  $R_{ct}$  represents charge transfer resistance. A CPE can be described by the following equation [28-30]:

$$Z_{\text{CPE}} = \frac{1}{Y_0(j\omega)^n} \quad (1)$$

where  $Y_0$  is a proportionality coefficient,  $\omega$  is the angular frequency ( $\omega=2\pi f$ , where  $f$  is the AC frequency), and  $j$  is the imaginary unit. The constant  $n$  is the CPE exponent (phase shift), which can be explained as a degree of surface in homogeneity [31]. While the CPE represents a pure capacitor,  $n=1$ , for  $n=-1$ , an inductor, and for  $n=0$ , a pure resistor. The capacitance values ( $C_{\text{dl}}$ ) and adsorption efficiency ( $Q_{\text{E}}$ ) can be calculated as follow:

$$C_{\text{dl}} = \frac{Y_0\omega^{n-1}}{\sin(n\pi/2)} \quad (2)$$

$$Q_{\text{E}} = \frac{R_{\text{ct}}^* - R_{\text{ct}}^0}{R_{\text{ct}}^*} \times 100\% \quad (3)$$

where  $R_{\text{ct}}^0$  and  $R_{\text{ct}}^*$  are the charge transfer resistance without and with KX (X=Cl, Br, I), respectively. The obtained impedance parameters such as  $R_{\text{s}}$ ,  $R_{\text{ct}}$ ,  $Y_0$ , and  $n$  were collected in Table 2.

**Table 2.** Impedance parameters of mild steel in 0.5 M H<sub>2</sub>SO<sub>4</sub> in the presence and absence of  $5 \times 10^{-3}$  M KX (X=Cl, Br, I).

Species	$R_{\text{s}} (\Omega \text{ cm}^2)$	CPE		$R_{\text{ct}} (\Omega \text{ cm}^2)$	$C_{\text{dl}} (\mu\text{F cm}^{-2})$	$Q_{\text{E}} (\%)$
		$Y_0 (\times 10^{-5} \text{ S s}^n \text{ cm}^{-2})$	$n$			
Blank	0.136	67.9	0.872	20.78	475	/
KCl	0.173	61.6	0.863	33.38	437	37.7
KBr	0.129	46.7	0.876	51.54	355	59.6
KI	0.094	22.0	0.850	181.0	207	88.5

As presented in Table 2, the  $R_{\text{ct}}$  values increased prominently after the addition of KX, which can be attributed to the adsorption of halide ions on iron surface. Consequently, an insulating layer was formed and the mass or charge-transfer at the electrode surface was blocked [32]. The adsorption efficiency orders are  $\Gamma^- > \text{Br}^- > \text{Cl}^-$  with the highest  $Q_{\text{E}}$  value of 88.5% for KI. Then one can draw a conclusion that  $\Gamma^-$  ions are more predisposed to adsorption than  $\text{Br}^-$  and  $\text{Cl}^-$  ions. It also means that  $\Gamma^-$  ions have a low degree of hydration and thus can be adsorbed preferentially on the metal surface [33]. There was not significant change in the value of the phase shift  $n$ , the ongoing stability of  $n$  between 0.850 and 0.876 indicates that the charge transfer process always controls the anodic dissolution of mild steel in 0.5 M H<sub>2</sub>SO<sub>4</sub> solution whether KX exists or not, and the  $C_{\text{dl}}$  values are in reasonable confidence limit. However, we can see that the  $C_{\text{dl}}$  values decrease in the presence of halide ions. This phenomenon can be interpreted through the Helmholtz model, in which the  $C_{\text{dl}}$  is very sensitive to the surface changes as given in the following formula [34-36]:

$$C_{\text{dl}} = \frac{\epsilon_0 \epsilon A}{d} \quad (4)$$

where  $\epsilon_0$  is the permittivity of the air,  $\epsilon$  is the local dielectric constant of the medium,  $d$  is the thickness of the protective film, and  $A$  is the electrode surface area. Therefore, the decrease in  $C_{\text{dl}}$  is resulted from the decrease in the  $\epsilon$  value and/or an increase in the thickness  $d$ , indicating that the halide

ions are adsorbed on the iron/solution interface at the corrosion potential by replacing the water molecules.

### 3.2. Polarization measurements

The potentiodynamic curves obtained for the mild steel electrode in 0.5 M H<sub>2</sub>SO<sub>4</sub> solution with and without 5×10<sup>-3</sup> M KX were shown in Figure 5. Some polarization parameters, for instance, corrosion potential ( $E_{\text{corr}}$ ), corrosion current density ( $i_{\text{corr}}$ ), cathodic and anodic tafel slopes ( $\beta_c$ ,  $\beta_a$ ) were collected in Table 3. The  $i_{\text{corr}}$  values were determined by extrapolation of the linear segments of the anodic and cathodic Tafel regions to the corrosion potential. Therefore, the adsorption efficiency ( $Q_p$ ) was calculated using the following equation:

$$Q_p = \frac{i_{\text{corr}}^0 - i_{\text{corr}}^*}{i_{\text{corr}}^0} \times 100\% \quad (5)$$

where  $i_{\text{corr}}^0$  and  $i_{\text{corr}}^*$  are the corrosion current density of mild steel in the absence and presence of inhibitors, respectively.

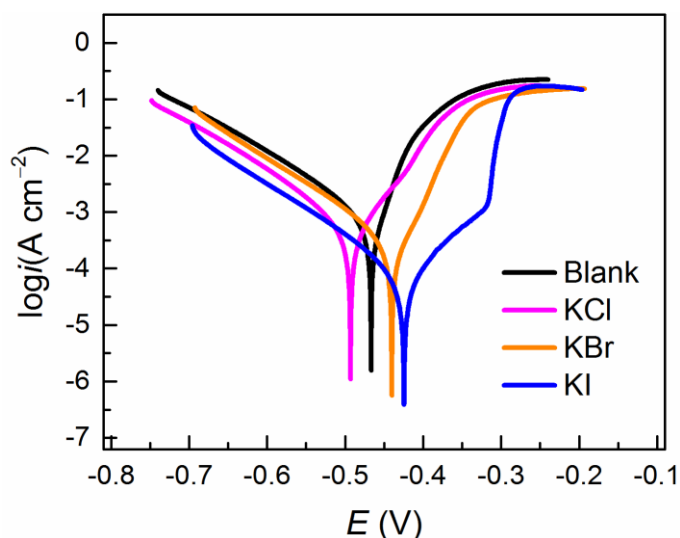


**Figure 5.** Potentiodynamic polarization curves for mild steel in 0.5 M H<sub>2</sub>SO<sub>4</sub> in the absence and presence of 5 × 10<sup>-3</sup> M KX (X=Cl, Br, I).

Based on the results in Table 3 and Figure 5, we find that the cathodic  $i$ - $E$  curves showed parallel Tafel lines indicating that the hydrogen evolution reaction is activation-controlled. The addition of KX does not change the values of cathodic Tafel slope ( $\beta_c$ ). The  $\beta_c$  values are approximately equal to 0.10 V dec<sup>-1</sup>. These results demonstrated that both the anodic dissolution as well as cathodic hydrogen evolution reaction were inhibited, and the adsorption efficiency of anion increased from KCl to KI, reaching a maximum value of 89.5%. Obviously, the corrosion mechanism of mild steel is not disrupted when the halide ions exist. It is worth noting that the adsorption

efficiencies calculated from potentiodynamic polarization measurements show the same trend as that obtained from EIS tests. This implies that our test results have a certain reliability.

**Table 3.** Potentiodynamic polarization parameters for mild steel in 0.5 M H<sub>2</sub>SO<sub>4</sub> with and without KX (X=Cl, Br, I).

Species	$E_{\text{corr}}$ (mV)	$i_{\text{corr}}$ ( $\mu\text{A cm}^{-2}$ )	$\beta_c$ (V dec <sup>-1</sup> )	$\beta_a$ (V dec <sup>-1</sup> )	$Q_p$ (%)
Blank	-466	721	0.105	0.041	/
KCl	-493	483	0.097	0.055	33.1
KBr	-441	286	0.099	0.042	55.6
KI	-424	75.3	0.098	0.059	89.5

### 3.3. Monte Carlo simulation

To further understand the adsorption mechanism of halogen ions on iron surface, a rigorous modeling of the direct interaction between the halogen ions and Fe(110) surface was carried out by Monte Carlo simulation. It helps to predict the most stable adsorption sites on metal surface.

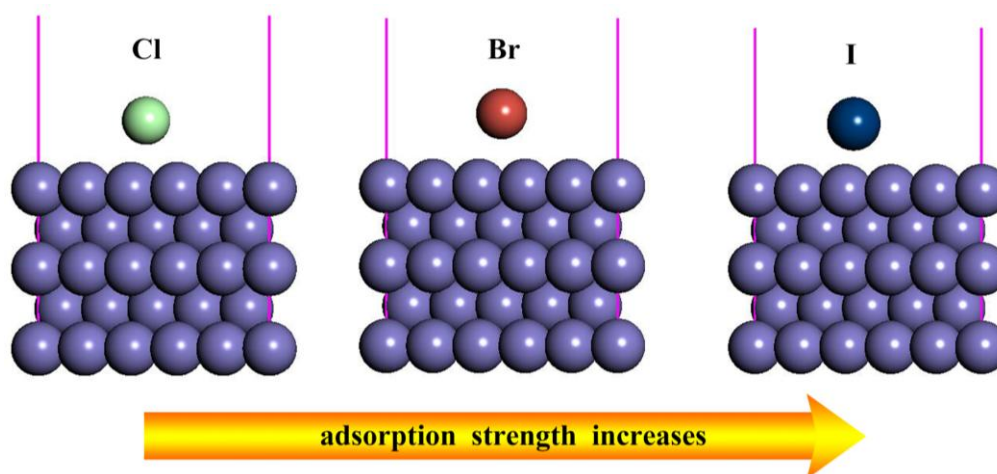


**Figure 6.** Side view of the most stable low energy configurations for the adsorption of X<sup>-</sup> (X=Cl, Br, I) ions on Fe(110) surface.

The equilibrium configurations of the X<sup>-</sup>/Fe(110) systems are shown in Figure 6. The distances between the halogen atoms and the first layer iron atoms are in the range of 3 to 4 Å for three investigated systems, which demonstrates that there exists a rather weak electrostatic interaction as well as van der Waals force between iodine ions and Fe(110) surface, and the former is predominant. Generally, adsorption energy ( $E_{\text{ads}}$ ) is defined as the energy released (or required) during the adsorption of the flexible adsorbate components on the substrate. Higher negative adsorption energy values suggest a more stable and stronger interaction between the adsorbate and metal substrate [20,

37]. The observed adsorption energy distribution of  $X^-$  ( $X=Cl, Br, I$ ) ions on Fe(110) surface are given in Figure 7. It can be seen from the results that the magnitude of  $E_{ads}$  for  $X^-$  ( $X=Cl, Br, I$ ) ions on Fe(110) surface was found to be in the following sequence  $\Gamma > Br^- > Cl^-$ , which is in good agreement with the above mentioned experimental findings. The adsorption density of three halide ions on the Fe(110) substrate has been presented in Figure 8. Obviously, the studied ions are likely to adsorb on the iron surface to form stable adsorption layers and protect iron from corrosion.

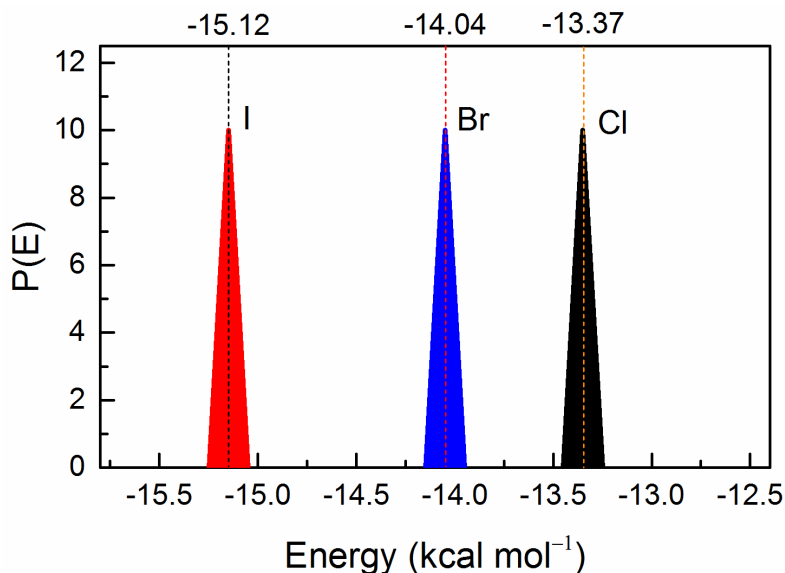


**Figure 7.** The adsorption energy distribution of the adsorbate  $X^-$  ( $X=Cl, Br, I$ ) ions on Fe(110) surface.

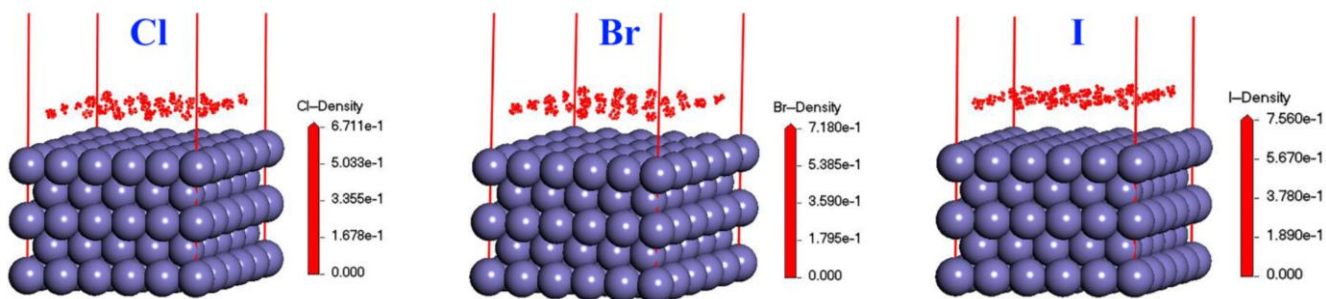


**Figure 8.** The adsorption density field of  $X^-$  ( $X=Cl, Br, I$ ) ions on Fe(110) substrate.

#### 4. CONCLUSIONS

Specific adsorption of anions is a common phenomenon in the field of metal/solution interface. In this work, the adsorption behavior of three typical halide ions, *i.e.*,  $Cl^-$ ,  $Br^-$ ,  $I^-$ , on iron surface in acid medium have been systematically investigated through electrochemical and theoretical calculation methods. The EIS and Tafel findings are basically in well agreement with MC simulation results. The main conclusions in this paper are as follows:

(1) Both the hydrogen evolution and the mild steel dissolution reactions were inhibited due to the adsorption of halide ions on iron/acid interface.

(2) The adsorption ability of halide ions on the iron surface has been estimated in the order:  $\text{I}^- > \text{Br}^- > \text{Cl}^-$ .

(3) A weak physisorption may exist between the halide atoms and iron surface atoms.

#### ACKNOWLEDGEMENTS

This research was sponsored by the Science and Technology Program of Guizhou Province (QKHJC2016-1149), the Guizhou Provincial Department of Education Foundation (QJHKYZ2016-105, 2016-009), the Opening Project of Material Corrosion and Protection Key Laboratory of Sichuan Province (2016CL06), the Guizhou Provincial Department of Education 125 Major Project Foundation (QJH2013-027), the Research Fund for the Doctoral Program of Tongren University (trxyDH1510), the Student's Platform for Innovation and Entrepreneurship Training Program (2016106665), and the Scientific and Technological Research Program of Chongqing Municipal Education Commission (KJ1500910, KJ1500942).

#### References

1. P. R. Mussini, S. Ardizzone, G. Cappelletti, M. Longhi, S. Rondinini and L. M. Doubova, *J. Electroanal. Chem.*, 552 (2003) 213.
2. F. J. Hingston, R. J. Atkinson, Posner, A. M. Amp and J. P. Quirk, *Nature*, 215 (1967) 1459.
3. N. A. Rogozhnikov, *Russ. J. Electrochem.*, 44 (2008) 198.
4. B. S. Hoener, C. P. Byers, T. S. Heiderscheit, A. S. De Silva Indrasekara, A. Hoggard, W. S. Chang, S. Link and C. F. Landes, *J. Phys. Chem. C*, 120 (2016) 20604.
5. D. Larkin, K. L. Guyer, J. T. Hupp and M. J. Weaver, *J. Electroanal. Chem.*, 138 (1982) 401.
6. S. Toshima and I. Uchida, *Electrochim. Acta*, 15 (1970) 1717.
7. T. H. Ha, H. J. Koo and B. H. Chung, *J. Phys. Chem. C*, 111 (2007) 1123.
8. I. Hwang, E. Ahn and Y. Tak, *Int. J. Electrochem. Sci.*, 9 (2014) 5454.
9. L. Guo, G. Ye, I. B. Obot, X. Li, X. Shen, W. Shi and X. Zheng, *Int. J. Electrochem. Sci.*, 12 (2017) 166.
10. A. Y. Musa, A. Mohamad, A. A. H. Kadhum, M. S. Takriff and L. T. Tien, *Corros. Sci.*, 53 (2011) 3672.
11. G. Eyu, G. Will, W. Dekkers and J. MacLeod, *Materials*, 9 (2016) 868.
12. X. M. Wang, Y. Wan, Q. Wang and Y. Ma, *Int. J. Electrochem. Sci.*, 8 (2013) 806.
13. I. Lozano, E. Mazario, C. O. Olivares-Xometl, N. V. Likhanova and P. Herrasti, *Mater. Chem. Phys.*, 147 (2014) 191.
14. G. Ji, P. Dwivedi, S. Sundaram and R. Prakash, *Ind. Eng. Chem, Res.*, 52 (2013) 10673.
15. L. Guo, S. Zhu and S. Zhang, *J. Ind. Eng. Chem.*, 24 (2015) 174.
16. X. W. Zheng, S. T. Zhang, W. P. Li, L. L. Yin, J. H. He and J. F. Wu, *Corros. Sci.*, 80 (2014) 383.
17. R. L. C. Akkermans, N. A. Spenley and S. H. Robertson, *Mol. Simul.*, 39 (2013) 1153.
18. J. H. Tan, L. Guo, T. M. Lv and S. T. Zhang, *Int. J. Electrochem. Sci.*, 10 (2015) 823.
19. I. B. Obot, S. Kaya, C. Kaya and B. Tüzün, *Res. Chem. Intermed.*, (2015).
20. K. F. Khaled and A. El-Maghraby, *Arab. J. Chem.*, 7 (2014) 319.
21. C. Verma, M. A. Quraishi, K. Kluza, M. Makowska-Janusik, L. O. Olasunkanmi and E. E. Ebenso, *Sci. Rep.*, 7 (2017) 44432.
22. H. Sun, Z. Jin, C. Yang, R. L. Akkermans, S. H. Robertson, N. A. Spenley, S. Miller and S. M. Todd, *J Mol Model*, 22 (2016) 47.
23. L. Guo, I. B. Obot, X. Zheng, X. Shen, Y. Qiang, S. Kaya and C. Kaya, *Appl. Surf. Sci.*, 406

- (2017) 301.
24. S. S. Abdel-Rehim, K. F. Khaled and N. S. Abd-Elshafi, *Electrochim. Acta*, 51 (2006) 3269.
  25. R. X. Chen, L. Guo and S. Y. Xu, *Int. J. Electrochem. Sci.*, 9 (2014) 6880.
  26. M. M. Solomon and S. A. Umoren, *J. Colloid Interface Sci.*, 462 (2016) 29.
  27. V. V. Pototskaya and O. I. Gichan, *Electrochim. Acta*, 235 (2017) 583.
  28. S. A. Ali, M. T. Saeed and S. U. Rahman, *Corros. Sci.*, 45 (2003) 253.
  29. M. Hosseini, S. F. L. Mertens, M. Ghorbani and M. R. Arshadi, *Mater. Chem. Phys.*, 78 (2003) 800.
  30. Y. Zhou, L. Guo, S. Zhang, S. Kaya, X. Luo and B. Xiang, *RSC Adv.*, 7 (2017) 23961.
  31. Y. Qiang, S. T. Zhang, S. Y. Xu, L. Guo, N. X. Chen and I. B. Obot, *Int. J. Electrochem. Sci.*, 11 (2016) 3147.
  32. Y. Sangeetha, S. Meenakshi and C. S. Sundaram, *Carbohydr. Polym.*, 136 (2016) 38.
  33. L. A. Al Juhaiman, A. Abu Mustafa and W. K. Mekhamer, *Anti-Corros. Method. M.*, 60 (2013) 28.
  34. P. Singh, E. E. Ebenso, L. O. Olasunkanmi, I. B. Obot and M. A. Quraishi, *J. Phys. Chem. C*, 120 (2016) 3408.
  35. M. Prabakaran, S. H. Kim, V. Hemapriya and I. M. Chung, *J. Ind. Eng. Chem.*, 37 (2016) 47.
  36. Z. Zhang, N. Tian, W. Zhang, X. Huang, L. Ruan and L. Wu, *Corros. Sci.*, 111 (2016) 675.
  37. K. F. Khaled, N. S. Abdelshafi, A. A. El-Maghraby, A. Aouniti, N. Al-Mobarak and B. Hammouti, *Int. J. Electrochem. Sci.*, 7 (2012) 12706.

© 2017 The Authors. Published by ESG ([www.electrochemsci.org](http://www.electrochemsci.org)). This article is an open access article distributed under the terms and conditions of the Creative Commons Attribution license (<http://creativecommons.org/licenses/by/4.0/>).